A FAST MULTIGRID ALGORITHM FOR ENERGY MINIMIZATION UNDER PLANAR DENSITY CONSTRAINTS

DORIT RON *, ILYA SAFRO [†], AND ACHI BRANDT [‡]

Abstract. The two-dimensional layout optimization problem reinforced by the efficient space utilization demand has a wide spectrum of practical applications. Formulating the problem as a nonlinear minimization problem under planar equality and/or inequality density constraints, we present a linear time multigrid algorithm for solving correction to this problem. The method is demonstrated on various graph drawing (visualization) instances.

Key words. Multigrid methods; Optimization, Inequality constraints, Models, numerical methods; Layout problems

AMS subject classifications. 65M55, 80M50, 65C20

1. Introduction. The optimization problem addressed in this paper is to find an optimal layout of a set of two-dimensional objects such that (a) the total length of the given connections between these objects will be minimal, (b) the overlapping between objects will be as little as possible, and, (c) the two-dimensional space will be well used. This class of problems can be modelled by a graph in which every vertex has a predefined shape and area and each edge has a predefined weight. While the first two conditions are straightforward, the third requirement can be made concrete in different ways. To see its usefulness, consider for example, the problem of drawing the "snake"-like graph shown in Figure 1(a). Most graph drawing algorithms would draw it as a line or a chord. In that case, when the number of nodes is big, the space is used very inefficiently, and the size of the nodes must decrease. One possible efficient space utilization for the graph "snake" is presented in Figure 1(b).
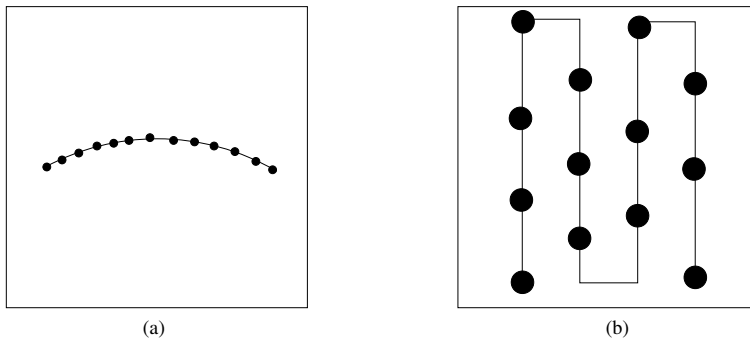

(a)   (b)

FIG. 1.1. *Possible ways to draw the "snake"-like graph: (a) when the drawing area is not used, the size of the nodes must decrease; and (b) a clearer picture is obtained when the space is used efficiently.*

In many theoretical and industrial fields, this class of problems is often addressed and actually poses a computational bottleneck. In this work we present a multilevel solver for a model that describes the core part of those applications, namely, the problem of minimizing a quadratic energy functional under planar constraints that

---

*The Weizmann Institute of Science, dorit.ron@weizmann.ac.il

[†]Argonne National Laboratory, safro@mcs.anl.gov

[‡]The Weizmann Institute of Science

bound the allowed amount of material (total areas of objects) in various subdomains of the entire domain under consideration.

Given an initial arrangement, the main contribution of this work is to enable a *fast* rearrangement of the entities under consideration into a more evenly distributed state over the entire defined domain. This process is done by introducing a sequence of finer and finer grids over the domain and demanding at each scale *equidensity*, that is, meeting equality or inequality constraints at each grid square, stating how much material it may (at most) contain. Since many variables are involved and since the needed updates may be large, we introduce a new set of *displacement* variables attached to the introduced grid points, which enables *collective* moves of many original variables at a time, at different scales including large displacements. The use of such multiscale moves has two main purposes: to enable processing in various scales and to *efficiently* solve the (large) system of equations of energy minimization under equidensity demands. The system of equations of the finer scales, when many unknowns are involved, is solved by a combination of well-known multigrid techniques (see [3, 4, 14]), namely, the *Correction Scheme* for the energy minimization part and the *Full Approximation Scheme* for the inequality equidensity constraints defined over the grid's squares. We assume here that the minimization energy functional has a quadratic form, but other functionals can be used via quadratization. The entire algorithm solves the nonlinear minimization problem by applying successive steps of corrections, each using a linearized system of equations.

Clearly, for each specific application, one has to tune the general algorithm to respect the particular task at hand. We have chosen here to demonstrate the performance of our solver on some instances of the graph visualization problem showing the efficient use of the given domain. Let us review a few applications that have motivated our research.

Graph visualization addresses the problem of constructing a geometric representation of graphs and has important applications to many technologies. There are many different demands for graph visualization problems, such as draw a graph with a minimum number of edge crossings, or a minimum total edge length, or a predefined angular resolution (for a complete survey, see [2]). The ability to achieve a compact picture (without overlapping) is of great importance, since area-efficient drawings are essential in practical visualization applications where screen space is one of the most valuable commodities. One of the most popular strategies that does address these questions is the force directed method [7] which has a quadratic running time if all pairwise vertex forces are taken into account. There are several successful multilevel algorithms [10] developed to improve the method's complexity. However, reducing the running time in these models usually means a loss of information regarding those forces.

Representation of higraphs. Higraphs, a combination and extension of graphs and Euler/Venn diagrams, were defined by Harel in [9]. Higraphs extend the basic structure of graphs and hypergraphs to allow vertices to describe inclusion relationships. Adjacency of such vertices is used to denote set-theoretic Cartesian products. Higraphs have been shown to be useful for the expression of many different semantics and underlie many visual languages, such as statecharts and object model diagrams. The well-known force-directed method has been extended to enable handling the visualization of higraphs [8]. For small higraphs it has indeed yielded nice results; but because of its high complexity, it poses efficiency challenges when used for larger higraphs.

Facility location problem. In this class of problems the goal is to locate a number of facilities within a minimized distance from the clients. In many industrial versions of the problem there exist additional demands such as the minimization of the routing between the facilities and various space constraints (e.g., the factory planning problem) while given a total area on which the facilities and clients could be located (for a complete survey, see [6]).

Wireless networks and coverage problems have a broad range of applications in the military, surveillance, environment monitoring, and healthcare fields. In these problems, having a limited number of resources (like antenna or sensor), one has to cover the area on which many demand points are distributed and have to be serviced. In many practical applications there are predefined connections between these resources that can be modeled as a graph [12, 5, 11].

The placement problem. The electronics industry has achieved a phenomenal growth over the past two decades, mainly due to the rapid advances in integration technologies and large-scale systems design - in short, due to the advent of VLSI. The number of applications of integrated circuits in high-performance computing, telecommunications, and consumer electronics has been rising steadily, and at a very fast pace. Typically, the required computational power of these applications is the driving force for the fast development of this field. The global placement is one of the most challenging problems during VLSI layout synthesis. In this application the modules must be placed in such a way that the chip can be processed at the detailed placement stage and then routed efficiently under many different constraints. This should be accomplished in a reasonable computation time even for circuits with millions of modules since it is one of the bottlenecks of the design process. For a most recent survey of the placement techniques see [13].

The paper is organized as follows. The problem definition is described in Section 2. The multilevel formulation and solver are presented in Section 3. Examples of graph drawing layout corrections are demonstrated in Section 4.

2. Problem definition. Given a weighted undirected graph $G = (V, E)$, let $v(i) > 0$ be the (rectangular) area of vertex (node) $i \in V$, $i = 1, ..., |V|$, and w_{ij} the non-negative weight of the edge ij between nodes i and j ($w_{ij} = 0$ if $ij \notin E$). Also, assume a twodimensional *initial* layout is given; that is, the center of mass of node i is considered to be located at $(\tilde{x}_i, \tilde{y}_i)$ within a given rectangular domain. The purpose of the optimization problem we consider is to modify the initial assignment $(\tilde{x}, \tilde{y})$ by (δ_x, δ_y) so as to minimize the quadratic functional

$$\mathfrak{E}(\delta_x, \delta_y) = \frac{1}{2} \sum_{ij \in E} w_{ij} \left((\tilde{x}_i + \delta_{x_i} - \tilde{x}_j - \delta_{x_j})^2 + (\tilde{y}_i + \delta_{y_i} - \tilde{y}_j - \delta_{y_j})^2 \right) , \qquad (2.1)$$

subject to some *equidensity* demands on the area distribution of the nodes within the given rectangle. To apply such constraints, we discretize the domain by a standard grid $\mathcal{G}$ consisting of a set of squares $\mathcal{S}(\mathcal{G})$, where each square $s \in \mathcal{S}(\mathcal{G})$ is of area $\mathcal{A} = h_x h_y$ and h_x and h_y are the mesh sizes of $\mathcal{G}$ in the x and y directions, respectively (see Figure 2.1). Denote by $\Upsilon(s)$ the total area of the vertices overlapping with the square s; that is, $\Upsilon(s)$ is the sum over all the nodes coinsiding with s, each contributing the (possibly partial) area that overlaps with s (see Figure 2.2).

The *planar* constraints (i.e., the constraints that are distributed over the 2D plane, where each constraint defines a demand regarding some bounded area) can then simply state how much area is required to be in every square; that is, for each
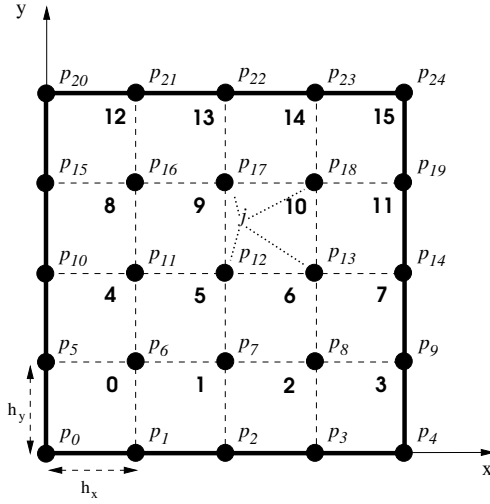
FIG. 2.1. *Example of a grid $\mathcal{G}$ with 25 grid points and 16 squares. The grid points and squares are labeled by p_i and bold numbers, respectively.*
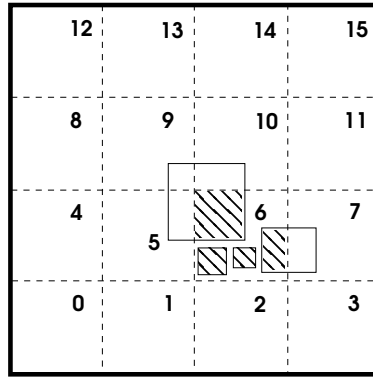

FIG. 2.2. *Example of $\Upsilon(s)$ for square 6. The total area of vertices overlapping with square 6 is dashed.*

square $s \in \mathcal{S}(\mathcal{G})$ the constraint is either $\Upsilon(s) = M(s)$, or $\Upsilon(s) \leq M(s)$, where $M(s)$ is the amount of nodes area desired or allowed for square s.

The constrained optimization problem with equality or inequality formulation can thus be summarized by the following

$$\begin{aligned} &\textbf{minimize} \quad \mathfrak{E} \quad \text{(given by (2.1))} \\ &\textbf{subject to} \quad \Upsilon(s) = (\leq)M(s) \; , \; \forall s \in \mathcal{S}(\mathcal{G}). \end{aligned} \qquad (2.2)$$

3. The multilevel formulation and solver. The aim of the current work is to provide a *fast* first-order correction to the given approximate solution; that is, we are looking for such a displacement that would in some optimal sense (to be defined below) improve the planar equidensity demands and/or decrease $\mathfrak{E}$. (Note that unconstrained minimization of $\mathfrak{E}$ will bring all nodes to overlap at a single point, and thus we may often observe an *increase* in $\mathfrak{E}$ upon removing some of the initial overlap.)

To enable a direct use of the multigrid paradigm, and motivated by the need to

perform *collective* moves of nodes (as explained in the introduction), we have actually reformulated the problem (2.1) as described in Section 3.1. The multilevel solver of the (reformulated) system (3.10) below is introduced in Section 3.2. This system of equations actually has to be solved for a *sequence* of different grid sizes to enhance the overall equidensity for a variety of scales as presented in Section 3.3.

3.1. Formulation of the correction problem. We have first introduced two new sets of variables u and v that correspond to *displacements* in the horizontal and vertical directions, respectively. These variables are located at the *grid points* $\mathcal{P}(\mathcal{G})$ which are sequentially counted from 0 to $|\mathcal{P}(\mathcal{G})|-1$ as shown in Figure 2.1. Each point $p \in \mathcal{P}(\mathcal{G})$ is associated with two variables u_p and v_p that influence the displacements of all the nodes located in the (up to four) squares intersecting at p. For example, the horizontal update of (the center of mass of) node j, depicted in Figure 2.1, is obtained from points p_{12}, p_{13}, p_{17} and p_{18}:

$$x_j \leftarrow x_j + \alpha_{12,j} u_{12} + \alpha_{13,j} u_{13} + \alpha_{17,j} u_{17} + \alpha_{18,j} u_{18},$$

where $\alpha_{12}, \alpha_{13}, \alpha_{17}$ and α_{18}, are the standard bilinear interpolation coefficients (their sum equals 1). The vertical coordinate y_j is updated from the v variables using the *same* coefficients.

For a node i denote the set of four closest points in $\mathcal{P}(\mathcal{G})$ (the corners of the square its center of mass is located at) by $c(i)$. The new quadratic energy functional we would like to minimize for u and v given a current layout $(\tilde{x}, \tilde{y})$ of G (i.e., the coordinates of node i are initialized with $(\tilde{x}_i, \tilde{y}_i)$) is

$$\mathfrak{E}(u, v) =$$
$$\frac{1}{2} \sum_{ij \in E} w_{ij} \left[\left(\tilde{x}_i + \sum_{p \in c(i)} \alpha_{pi} u_p - \tilde{x}_j - \sum_{p \in c(j)} \alpha_{pj} u_p \right)^2 + \left(\tilde{y}_i + \sum_{p \in c(i)} \alpha_{pi} v_p - \tilde{y}_j - \sum_{p \in c(j)} \alpha_{pj} v_p \right)^2 \right],$$
$$(3.1)$$

where α_{pi} are the bilinear interpolation coefficients.

The reformulation of the equidensity constraint in terms of the displacement variables relies on the rule of conservation of areas. The initial total amount of vertex areas at each square equals the current actual amount of areas dictated by $(\tilde{x}, \tilde{y})$. To estimate the amount of areas flowing inside and outside a given square induced by the u and v displacements, we assume the nodes are evenly distributed inside the squares. Under this assumption it is easier to estimate the amount of area being transferred between two adjacent squares as explained below. Consider, for example, a square s. Denote by $\Upsilon_{r(l,t,b)}(s)$ the total area of nodes overlapping with its *right (left, top, bottom) neighbor* square. Let $u_{rt(rb,lt,lb)}(s)$ be the u values at the *right-top (right-bottom, left-top, left-bottom)* corner of s as shown in Figure 3.1. To estimate the amount of areas entering s from the right we first calculate the average area (per squared unit) in *both* squares: $(\Upsilon(s) + \Upsilon_r(s))/2\mathcal{A}$. We have to multiply this by the actual entering area (of nodes), which is a rectangle of height h_y, the length of the border between the two squares, and width, which is the average of the u displacement at the middle of that border, namely, $(u_{rt} + u_{rb})/2$. Thus the overall contribution of area from the right is approximated by

$$\frac{\Upsilon(s) + \Upsilon_r(s)}{2\mathcal{A}} \cdot h_y \cdot \frac{u_{rt}(s) + u_{rb}(s)}{2} \qquad .$$

A similar term is calculated at the left, and with v instead of u also at the top and bottom. Note that if the assumed direction of flow is wrong the resulting displacement will just turn out to be negative.

The entire constraint for a square s stating that the net flow of areas into the square should be equal to or be smaller than some demand $M(s)$ minus the current area in u, is given below:

$$\mathfrak{eqd}(s) = \frac{\Upsilon(s) + \Upsilon_r(s)}{2\mathcal{A}} h_y \frac{u_{\mathrm{rt}}(s) + u_{\mathrm{rb}}(s)}{2} - \frac{\Upsilon(s) + \Upsilon_l(s)}{2\mathcal{A}} h_y \frac{u_{\mathrm{lt}}(s) + u_{\mathrm{lb}}(s)}{2} +$$
$$\frac{\Upsilon(s) + \Upsilon_t(s)}{2\mathcal{A}} h_x \frac{v_{\mathrm{rt}}(s) + v_{\mathrm{lt}}(s)}{2} - \frac{\Upsilon(s) + \Upsilon_b(s)}{2\mathcal{A}} h_x \frac{v_{\mathrm{rb}}(s) + v_{\mathrm{lb}}(s)}{2} \le M(s) - \Upsilon(s) \ .$$
$$(3.2)$$

Next, to enforce the natural boundary conditions on u and v, namely, to forbid flows across the external boundaries, we simply nullify all corresponding u_p on the right and left boundary points $\mathcal{B}_u(\mathcal{G})$, and v_p on the bottom and top boundary points $\mathcal{B}_v(\mathcal{G})$. Then the entire constrained optimization problem in terms of u and v and the initial approximation $(\tilde{x}, \tilde{y})$ is given by

$$
\begin{aligned}
\textbf{minimize} \quad & \mathfrak{E}(u,v) \quad \text{(given by (3.1)}\\
\textbf{subject to} \quad & \mathfrak{eqd}(s) = (\le) M(s) - \Upsilon(s) \ , \ \forall s \in \mathcal{S}(\mathcal{G}) \ ;\\
& \text{if } p \in \mathcal{B}_u(\mathcal{G}) \text{ then } u_p = 0 \ ;\\
& \text{if } p \in \mathcal{B}_v(\mathcal{G}) \text{ then } v_p = 0 \ .
\end{aligned}
\qquad (3.3)
$$

We will simplify the formulation of (3.3) by the concatenation of the two vectors u and v into one $\mathbf{u} = [\{u_i\}_{i=0}^{|\mathcal{P}(\mathcal{G})|-1} \mid \{v_i\}_{i=0}^{|\mathcal{P}(\mathcal{G})|-1}]$. We will also omit the boundary conditions by directly replacing all variables in $\mathcal{B}_u(\mathcal{G}) \cup \mathcal{B}_v(\mathcal{G})$ by 0, and so, from now on, we will refer to $\mathfrak{E}$ as

$$\mathfrak{E}(\mathbf{u}) = \frac{1}{2} \sum_{i,j} q_{ij} \mathbf{u}_i \mathbf{u}_j + \sum_i l_i \mathbf{u}_i + C \quad , \qquad (3.4)$$

where i, j run over all the indices in $\mathbf{u} \setminus \mathcal{B}_u(\mathcal{G}) \setminus \mathcal{B}_v(\mathcal{G})$, C is a constant and q_{ij}, l_i are the coefficients calculated directly from the previous definition (3.1) of $\mathfrak{E}$. Similarly rewrite each $\mathfrak{eqd}(s)$ in (3.2) as

$$\mathfrak{eqd}(s) = \sum_i a_{si} \mathbf{u}_i = (\le) b_s, \qquad (3.5)$$

where $b_s = M(s) - \Upsilon(s)$.

Denote by λ_s, $s \in \mathcal{S}(\mathcal{G})$ the Lagrange multiplier corresponding to the equidensity constraint of square s. If all the constraints are equality ones, the Lagrangian minimization functional is

$$\mathfrak{L}(\mathbf{u}, \lambda) = \mathfrak{E}(\mathbf{u}) + \sum_{s \in \mathcal{S}(\mathcal{G})} \lambda_s (\mathfrak{eqd}(s) - b_s) \quad . \qquad (3.6)$$

So, we are looking for a critical point of the Lagrangian function, which is expressed by the system of linear equations

$$\nabla \mathfrak{L}(\mathbf{u}, \lambda) = \begin{bmatrix} \nabla_{\mathbf{u}} \mathfrak{L}(\mathbf{u}, \lambda) \\ \nabla_\lambda \mathfrak{L}(\mathbf{u}, \lambda) \end{bmatrix} = 0 \quad . \qquad (3.7)$$

There are at least two factors that may cause (3.7) to be singular. First, the rank of $\nabla\mathfrak{L}(\mathbf{u}, \lambda)$ is always less than its size by at least 1. This arises from the equations of equidensity constraints in (3.7): their sum always equals zero. The reason is that under the boundary constraints the total amount of in-flows is always equal to the total amount of out-flows. In fact, the second summand in (3.6) can be replaced by
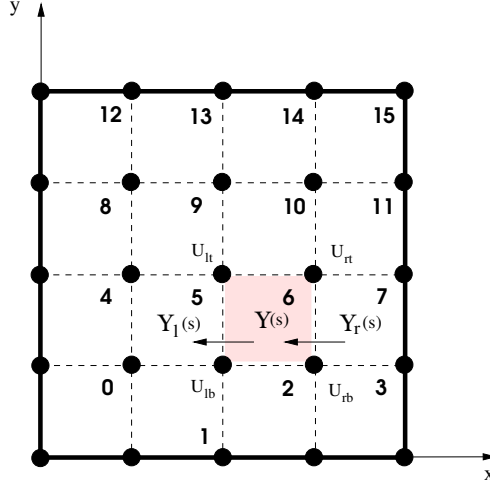

FIG. 3.1. *The horizontal direction flows of area considered for the square s (colored by gray) in the equidensity constraint (3.2).*

$$\sum_{s \in \mathcal{S}(\mathcal{G})} (\lambda_s + Z)(\mathfrak{eqd}(s) - b_s)$$

for any Z without changing the minimization of $\mathfrak{L}$ since

$$Z \sum_{s \in \mathcal{S}(\mathcal{G})} (\mathfrak{eqd}(s) - b_s) = 0 \ .$$

Thus, important are not the values of λ_s but only their *differences*, and the singularity can be treated by an additional constraint, say, $\sum_s d_s\lambda_s = 0$, where $d_s = 1 \ \forall s \in \mathcal{S}(\mathcal{G})$ (the introduction of d_s is necessary for the recursion of the multilevel solver; see Section 3.2.1). The additional term in $\mathfrak{L}(\mathbf{u}, \lambda)$ is $\eta \sum_s d_s\lambda_s$, where η is a "pseudo-Lagrange" multiplier. The following proposition (with $k = 1$) motivates the non-singularity of $\mathfrak{L}$ with $\sum_s d_s\lambda_s = 0$.

PROPOSITION 3.1. *Given a symmetric $n \times n$ matrix A, for which $rank(A) = n - k$, let x_i, $i = 1, ..., k$ be an orthgonal basis of the null space of A, that is, $Ax_i = 0$. Then the following block matrix B is nonsingular*

$$B = \left(\begin{array}{c|c} A & X \\ \hline X^T & 0 \end{array} \right) ,$$

where $X = (x_1, ..., x_k)$ is an $n \times k$ matrix of rank k.

Proof. Let y be any vector in $\mathbb{R}^{n+k}$. Denote by y' the first n components of y and by y'' the last k components, that is, $y = \left(\begin{array}{c} y' \\ y'' \end{array} \right)$. We will prove that if $By = 0$,

then $y = 0$. The vector By can be written in the following block form:

$$By = \left(\frac{Ay' + Xy''}{X^T y'} \right).$$

Multiplying $Ay' + Xy'' = 0$ by X^T from the left implies that $y'' = 0$, and hence $Ay' = 0$ and $y' = \sum_{i=1}^{k} \alpha_i x_i$. Substituting the last relation into each of the last k rows of B implies $x_j^T y' = x_j^T \sum_{i=1}^{k} \alpha_i x_i = \alpha_j x_j^T x_j = 0$ and thus $\alpha_j = 0$ for $j = 1, ..., k$ yielding $y' = 0$. Since $y' = 0$ and $y'' = 0$ we may conclude that $y = 0$ as needed. $\square$

The second kind of singularity in (3.7) may appear from possible empty squares. This can be treated by adding a summand to (3.6) that minimizes the total sum of all corrections $\beta \sum_i \mathbf{u}_i^2$, that is, adds a 2β-term to the diagonal of $\nabla_{\mathbf{u}} \mathfrak{L}$, where β is small enough to cause only negligible change in a solution. This will prevent the inclusion of zero-rows in $\nabla_{\mathbf{u}} \mathfrak{L}$, while possibly also bounding the size of each correction in the solver below.

To summarize, the pseudo-Lagrangian functional $\mathfrak{L}$ for our correction problem with equality constraint is

$$\mathfrak{L}(\mathbf{u}, \lambda, \eta) = \frac{1}{2} \sum_{i,j} q_{ij} \mathbf{u}_i \mathbf{u}_j + \sum_i l_i \mathbf{u}_i + \beta \sum_i \mathbf{u}_i^2 + \sum_{s \in \mathcal{S}(\mathcal{G})} \lambda_s (\sum_i a_{si} \mathbf{u}_i - b_s) + \eta \sum_{s \in \mathcal{S}(\mathcal{G})} d_s \lambda_s ,$$
(3.8)

leading to the following system of equations

$$\begin{array}{ll} \frac{1}{2} \sum_j q_{ij} \mathbf{u}_j + l_i + 2\beta \mathbf{u}_i + \sum_{s \in \mathcal{S}(\mathcal{G})} \lambda_s a_{si} = 0 , & \forall i \text{ s.t. } \mathbf{u}_i \in \mathbf{u} \setminus \mathcal{B}_u(\mathcal{G}) \setminus \mathcal{B}_v(\mathcal{G}) \\ \sum_i (a_{si} \mathbf{u}_i - b_s) + \eta d_s = 0 , & \forall s \in \mathcal{S}(\mathcal{G}) \\ \sum_{s \in \mathcal{S}(\mathcal{G})} d_s \lambda_s = 0 . & \end{array}$$
(3.9)

Since in real world situations the total area is usually *bigger* than the total area of all the vertices, the redefined minimization problem under *inequality* constraints will generally have the form

$$\begin{array}{lll} \textbf{minimize} & \mathfrak{E}(\mathbf{u}) & \text{(given by (3.4))} \\ \textbf{subject to} & \mathfrak{eqd}(s) \leq b_s , \ \forall s \in \mathcal{S}(\mathcal{G}) & \text{(given by (3.5))} . \end{array}$$
(3.10)

3.2. Multilevel solver for problem (3.10). To solve the constrained minimization problem (3.10), we use multigrid techniques: standard geometric coarsening, linear interpolation, Correction Scheme for the energy minimization and the Full Approximation Scheme for the equidensity inequality constraints; all are presented in Section 3.2.1. In addition, we have developed a fast window minimization relaxation as explained in Section 3.2.2. The multilevel cycle is schematically summarized in Section 3.2.3 in Algorithm **2D-layout-correction**.

3.2.1. Coarsening scheme. When the geometry of the problem is known we can choose a coarser grid by the usual elimination of every other line, as shown in Figure 3.2. The correction computed at the coarse grid points will be interpolated and added to the fine grid current approximation. Let us introduce the notation distinguishing between fine and coarse level variables and functions. By lowercase and uppercase letters we will refer to the variables, indexes, and coefficients of the fine ($\mathbf{u}_i$, i, q_j, etc.) and the coarse ($\mathbf{U}_I$, I, Q_J, etc.) levels, respectively. The subscripts f and c will be used to describe the energy $\mathfrak{E}_f$ and $\mathfrak{E}_c$ and pseudo-Lagrangian $\mathfrak{L}_f$ and $\mathfrak{L}_c$ functions at the fine and the coarse levels, respectively.
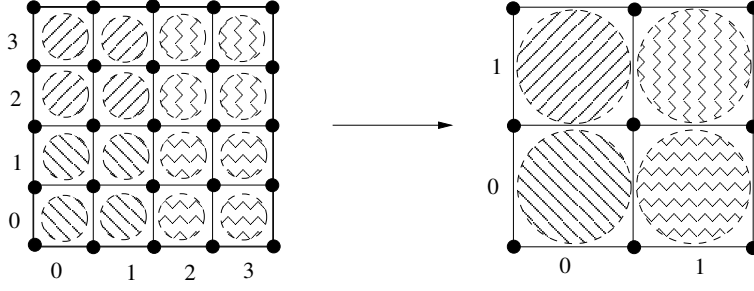
FIG. 3.2. *Geometric coarsening. The equidensity constraints of every four similarly patterned squares at the fine level form one equidensity constraint at the coarse level.*

Thus, the minimization part of the pseudo-Lagrangian (3.8) at the fine level is

$$\mathfrak{E}_f = \frac{1}{2} \sum_{ij} q_{ij} \mathbf{u}_i \mathbf{u}_j + \sum_i l_i \mathbf{u}_i \quad . \tag{3.11}$$

(Note that we have omitted the β term from the following derivation since it is merely an artificial added term.) Given a current approximation $\tilde{\mathbf{u}}$ of the fine level solution $\mathbf{u}$ and a correction function $\mathbf{U}$ calculated at the coarse level variables $\mathbf{U}$, $\tilde{\mathbf{u}}$ will be corrected by

$$\tilde{\mathbf{u}}_i \leftarrow \tilde{\mathbf{u}}_i + \sum_{I \ni i} \alpha_{iI} \mathbf{U}_I , \tag{3.12}$$

where the notation $\sum_{I \ni i}$ means that the sum is running over all coarse gridpoints p_I from which standard bilinear interpolation is made to the fine gridpoint p_i.

Expressing the fine level energy functional E_f in terms of the coarse variables by substituting (3.12) into (3.11) yields

$$\mathfrak{E}_f = \frac{1}{2} \sum_{ij} q_{ij} (\tilde{\mathbf{u}}_i + \sum_{I \ni i} \alpha_{iI} \mathbf{U}_I)(\tilde{\mathbf{u}}_j + \sum_{J \ni j} \alpha_{jJ} \mathbf{U}_J) + \sum_i l_i (\tilde{\mathbf{u}}_i + \sum_{I \ni i} \alpha_{iI} \mathbf{U}_I) =$$

$$= \frac{1}{2} \sum_{IJ} Q_{IJ} \mathbf{U}_I \mathbf{U}_J + \sum_I L_I \mathbf{U}_I + C ,$$

where $Q_{IJ} = \sum_{\substack{i \in I \\ j \in J}} q_{ij} \alpha_{iI} \alpha_{jJ}$, $L_I = \sum_{\substack{j \\ i \in I}} q_{ij} \tilde{\mathbf{u}}_j \alpha_{iI} + \sum_{i \in I} l_i \alpha_{iI}$ and C is a constant. Thus, the coarse level energy functional will be of the same structure as the fine level one, namely,

$$\mathfrak{E}_c = \frac{1}{2} \sum_{IJ} Q_{IJ} \mathbf{U}_I \mathbf{U}_J + \sum_I L_I \mathbf{U}_I .$$

For each fine square s the equidensity constraint $\mathfrak{eqd}(s)$ is given by (3.5). The coarse equidensity constraints are constructed by merging 2×2 fine squares into one coarse square S. The expression "$s \in S$" will refer to running over the four fine squares s that form the coarse square S (see Figure 3.2). The S-th planar equidensity constraint of the coarse level (in the case of equality constraints only) is obtained again by the substitution of (3.12):

$$\sum_{s \in S} \sum_i a_{si} \mathbf{u}_i - \sum_{s \in S} b_s = \sum_I A_{SI} \mathbf{U}_I - B_S ,$$

where $A_{SI} = \sum_{i \in I} \sum_{s \in S} a_{si} \alpha_{iI}$ and $B_S = \sum_{s \in S} (b_s - \sum_i a_{si} \tilde{\mathbf{u}}_i)$. Similarly (in the case of equality constraints), the additional η-constraint over all squares at the coarse level as inherited from the fine level is $\sum_S D_S \Lambda_S = 0$, where $D_S = \sum_{s \in S} d_s$.

To complete the description of the coarse equations, we still need to transfer the equidensity *inequality* constraints. For this purpose we will use the Full Approximation Scheme (FAS), which is the general multigrid strategy applied to nonlinear problems (see [3, 4, 14]). In fact, there is no need for the FAS for the equality equidensity constraints since it is a linear problem that can be solved by the regular Correction Scheme (CS). The FAS-like coarsening rules are needed and applied only on the set of equations derived from the equidensity inequalities. Thus, our scheme is a combination of the correction scheme for the energy equations derived from (3.11) and (3.12) and FAS-like rules for the equidensity equations.

To derive these equations we need to calculate the *residuals* for both the fine and coarse grids. If $\mathfrak{L}_f$ is the pseudo-Lagrangian of the fine level system defined by

$$\mathfrak{L}_f = \mathfrak{E}_f + \sum_s \lambda_s \left(\sum_i a_{si} \mathbf{u}_i - b_s \right) + \eta \sum_s d_s \lambda_s \quad , \tag{3.13}$$

where $\mathfrak{E}_f$ is given by (3.11), then the $\mathbf{u}_i$-th residual of $\nabla \mathfrak{L}_f$, where $\tilde{\lambda}_s$ is the current value of the Lagrange multiplier λ_s, is

$$r_i^{\mathfrak{E}} = -l_i - \frac{1}{2} \sum_j q_{ij} \tilde{\mathbf{u}}_j - \sum_s \tilde{\lambda}_s a_{si}.$$

Thus, the residual corresponding to the variable $\mathbf{U}_I$ of $\nabla \mathfrak{L}_c$ (where $\nabla \mathfrak{L}_c$ is the coarse level system of equations analogous to (3.13)) is

$$R_I^{\mathfrak{E}} = \sum_{i \in I} \alpha_{iI} r_i^{\mathfrak{E}} \quad , \tag{3.14}$$

where α_{iI} are as in (3.12); that is, the fine-to-coarse transfer is the adjoint of our coarse-to-fine interpolation. The residual of the s-th equidensity constraint is

$$r_s^{\mathfrak{eqd}} = b_s - \sum_i a_{si} \tilde{\mathbf{u}}_i - \tilde{\eta} d_s \quad ,$$

where s runs over all fine squares and $\tilde{\eta}$ is the current value of η. Therefore, the coarse equidensity residual of square S is

$$R_S^{\mathfrak{eqd}} = \sum_{s \in S} r_s^{\mathfrak{eqd}} \quad . \tag{3.15}$$

Finally the residual of the η-constraint is

$$r_\eta = -\sum_s d_s \tilde{\lambda}_s = R_H.$$

Denote by $LP(I)$ the linear part of the $\mathbf{U}_I$-th equation in the system $\nabla \mathfrak{L}_c$

$$LP(I) = \frac{1}{2} \sum_J Q_{IJ} \mathbf{U}_J + \sum_S \Lambda_S A_{SI}.$$

From the FAS rule for the I-th coarse equation stating that $LP(I) = R_I^{\mathfrak{E}} +$ the current approximation of $LP(I)$, we can derive the I-th $\nabla \mathfrak{L}_c$ equation

$$\frac{1}{2} \sum_J Q_{IJ} \mathbf{U}_J + \sum_S \Lambda_S A_{SI} - R_I^{\mathfrak{E}} - \frac{1}{2} \sum_J Q_{IJ} \mathbf{U}_J^0 - \sum_S \Lambda_S^0 A_{SI} = 0, \qquad (3.16)$$

where $R_I^{\mathfrak{E}}$ is given by (3.14), $\mathbf{U}_J^0 = 0$ and $\Lambda_S^0 = \frac{1}{4} \sum_{s \in S} \tilde{\lambda}_s$. Similarly, the S-th square coarse equation for the equality (inequality) constraint is

$$\sum_I A_{SI} \mathbf{U}_I + H D_S - R_S^{\mathfrak{eqd}} - \sum_I A_{SI} \mathbf{U}_I^0 - H^0 D_S = (\leq) 0 , \qquad (3.17)$$

where $R_S^{\mathfrak{eqd}}$ is given by (3.15). The last equation for the H-constraint is

$$\sum_S D_S \Lambda_S - R_H - \sum_S D_S \Lambda_S^0 = 0. \qquad (3.18)$$

Note that equations (3.16) to (3.18) are the coarse grid equations analog to the system (3.9). (A $2\beta \mathbf{U}_I$ term may be added to (3.16) for stability if needed.) The correction received from the coarse level for the $\mathbf{u}$ variables is given by (3.12) and for the Lagrange multipliers λ by

$$\tilde{\lambda}_s \leftarrow \tilde{\lambda}_s + \Lambda_{S \ni s} - \Lambda_{S \ni s}^0 . \qquad (3.19)$$

3.2.2. Relaxation. In our multigrid solver, as usual, the relaxation process is employed as the smoother of the error of the approximation, before the construction of the coarse level system and immediately after interpolation from the coarse level. For this purpose we have developed the *Window relaxation* procedure, which extracts from the entire system small subproblems of $m \times m$ squares and solves each separately, as explained below. The running time of the entire relaxation process strongly depends on the algorithm for solving one window. There exist many versions of well-known algorithms for the quadratic minimization problem under linear inequality constraints (for a survey see [1]). However, since each window need be solved only to a first approximation (because of the iterative nature of the overall algorithm), in order to keep the running time low, we have implemented a simple algorithm for approximately solving each single window, as presented in **SingleWindowSolver**.

Let $\mathcal{W} = \{s \in \mathcal{S}(\mathcal{G}) |$ all squares within an $m \times m$ super-square$\}$ be a window of squares. To solve the quadratic minimization problem in $\mathcal{W}$, we fix at their current position all $\mathbf{u}$ *outside* $\mathcal{W}$, as well as all those that are on the boundary of $\mathcal{W}$ and represent movement *perpendicular* to the boundary. The minimization is done under the set of equidensity constraints for the squares $s \in \mathcal{W}$. The solution process for each single window is a simplified version of the *active set method* and is iterative. At each iteration t, for a given $\tilde{\mathbf{u}}$ we first extract the set (denoted by S_t) of squares for which the respective inequality equidensity constraints are violated or almost violated:

$$S_t = \{s \in \mathcal{W} \mid \mathfrak{eqd}(s) > b_s - \epsilon\} ,$$

where ϵ is positive and sufficiently small but not too small to make S_t numerically unstable (we have used $\epsilon = 0.0001 * $(the square's area)). Then the inequality constraints of S_t are set to equalities ignoring the other inequality constraints. Let $\mathcal{P}_{\mathcal{W}}$ be the set of all displacement indexes inside $\mathcal{W}$ (including those on the boundary of

$\mathcal{W}$ directing *parallel* to it). For every $\mathbf{u}_i, i \in \mathcal{P}_\mathcal{W}$ we associate a correction variable δ_i and we reformulate the pseudo-Lagrangian for $\mathcal{W}$ as a functional of the δ_i variables as follows:

$$\mathfrak{L}_\mathcal{W}(\delta, \lambda) = \frac{1}{2} \sum_{i,j \in \mathcal{P}_\mathcal{W}} q_{ij}(\tilde{\mathbf{u}}_i + \delta_i)(\tilde{\mathbf{u}}_j + \delta_j) + \frac{1}{2} \sum_{i \in \mathcal{P}_\mathcal{W}, \ j \notin \mathcal{P}_\mathcal{W}} q_{ij}(\tilde{\mathbf{u}}_i + \delta_i)\tilde{\mathbf{u}}_j +$$

$$\sum_{i \in \mathcal{P}_\mathcal{W}} l_i(\tilde{\mathbf{u}}_i + \delta_i) + \beta \sum_{i \in \mathcal{P}_\mathcal{W}} (\tilde{\mathbf{u}}_i + \delta_i)^2 + \sum_{s \in S_t} \lambda_s \big(\sum_{i \in \mathcal{P}_\mathcal{W}} a_{si}\tilde{\mathbf{u}}_i - b_s \big) , \quad (3.20)$$

where $\tilde{\mathbf{u}}_i$ is the current value of $\mathbf{u}_i$ and the β term is added for stability with $\beta = 1$. Solving $\nabla \mathfrak{L}_\mathcal{W}(\delta, \lambda) = 0$ we obtain the corrections δ_i for $\tilde{\mathbf{u}}_i, i \in \mathcal{P}_\mathcal{W}$, which confine the respective active set variables to the boundary of the equality constraints manifold. However, while accepting this correction we may violate other inequality constraints that were already satisfied at the previous iteration $t - 1$. Let us call this set of new unsatisfied constraints $\overline{S}_t$. One way to overcome this problem is to accept only a *partial* correction $\theta\delta_i$, $i \in \mathcal{P}_\mathcal{W}$, where θ is the *smallest* number that brings some constraint from $\overline{S}_t$ to equality. Accepting the correction $\theta\delta_i$ does not violate any constraint from $\overline{S}_t$. At this point we accept this partial correction and continue to the next iteration $t+1$, excluding from the redefined S_t the set of satisfied (by equality) constraints from S_t with negative Lagrange multipliers λ_s.

SingleWindowSolver($\mathcal{W}$, $\tilde{\mathbf{u}}$)
begin
   $t = 0$
  Repeat until "optimal enough" (explained at the end of Section 4)
    If $t = 0$
        $S_t = \{$the violated equidensity constraints$\}$
    Else
        $S_t = \{$the violated equidensity constraints$\} \backslash$
            $\{$those from iteration $t - 1$ which satisfy equality and have $\lambda_s < 0\}$
    Solve $\nabla \mathfrak{L}_\mathcal{W}(\delta, \lambda) = 0$ and extract the smallest θ
    Accept the correction $\tilde{\mathbf{u}} \leftarrow \tilde{\mathbf{u}} + \theta\delta$
    $t \leftarrow t + 1$
end

To achieve corrections for all variables, we will cover by these windows the entire area in red-black order [14]. For computational reasons we have chosen to apply this relaxation for very small windows (of size 4×4 squares). To minimize the effects of the boundary constraints in the windows and to enforce the equidensity constraints over different super-squares, we scan the entire domain two more times: once with half-window size shift in the horizontal direction and once in the vertical. Thus the overall relaxation process covers the domain three times.

3.2.3. The multilevel cycle. Having defined the window relaxation, the interpolation, and the coarsening scheme, the multilevel cycle naturally follows. Starting from the given approximation $(\tilde{x}, \tilde{y})$, discretize the domain by a standard grid on which the $\mathbf{u}$ variables are initially defined. Construct the system of equations (3.9), and solve for the $\mathbf{u}$ variables as follows. After applying ν_1 window relaxation sweeps, define the coarser level equations for the coarser grid, apply ν_1 window relaxation sweeps there, and continue to a still coarser level. This process is recursively repeated

until a small enough problem is obtained. Solve this coarsest problem directly, and start the uncoarsening stage by interpolating the solution of the coarse level to the finer levels followed by ν_2 window relaxation sweeps on the finer level. Repeat until the correction to the original problem is obtained. This entire multilevel cycle, usually referred to as the *V-cycle*, is summarized in procedure **V-cycle-correction** below, where the superscript index refers to the level number. (We have used $\nu_1 = \nu_2 = 3$).

V-cycle-correction($\mathcal{G}^i$, $\mathbf{u}^i$, $\mathcal{C}^i$, λ^i, $\nabla\mathfrak{L}^i$)
begin
   If $\mathcal{G}^i$ is a small enough grid
     Solve the problem exactly
   Else
     Set $\mathbf{u}^i = 0$
     Apply ν_1 *Window relaxation* sweeps
     Construct $\mathcal{G}^{i+1}$ the coarse level grid
     Define $\mathcal{C}^{i+1}$ to be the set of equidensity constraints
     Initialize the system of equations $\nabla\mathfrak{L}^{i+1}$ given by (3.16)-(3.18)
     Initialize $\mathbf{u}^{i+1}$ and λ^{i+1}
     V-cycle-correction($\mathcal{G}^{i+1}$, $\mathbf{u}^{i+1}$, $\mathcal{C}^{i+1}$, λ^{i+1}, $\nabla\mathfrak{L}^{i+1}$)
     Interpolate from level $i + 1$ to level i using (3.12) and (3.19)
     Apply ν_2 *Windows relaxation* sweeps
Return $\mathbf{u}^i$

3.3. The Full MultiGrid external driving routine. The solution of (3.9) is primarily dependent on the chosen grid size. To enforce equidensity at all scales, it can be used within the Full MultiGrid (FMG) framework. This is done by using a *sequence* of increasing grid sizes (progressively finer meshsizes), while employing a small number of V-cycles for each grid size. We emphasize that the original problem (2.2) is highly nonlinear, while the system of equations with corrections in term of the displacement $\mathbf{u}$ is linearized around the current solution $(\tilde{x}, \tilde{y})$. Therefore, only a small correction should actually be taken from the $\mathbf{u}$ displacements when these $(\tilde{x}, \tilde{y})$ are being updated. Then, a new linear system can be formulated around the new solution to obtain a new correction, and so forth. Thus, by small steps of corrections we solve the original nonlinear problem via the corrections calculated from the linear system of equidensity constraints. For instance, we have tried to employ grids of sizes: 2, 4, 8, ... up to a grid with number of squares comparable to the number of nodes in the graph. For each grid size the corresponding set of equations (in terms of the displacement $\mathbf{u}$) is solved either directly (for small enough grids) or by employing the V-cycles described in Section 3.2.3. In either cases the obtained solution $\mathbf{u}$ is interpolated back to the (x, y) variables, introducing the desired correction to the original variables of the problem. Various driving routines can be actually used: each chosen grid size may be solved more than once (e.g., use grids 2, 2, 4, 4, 8,...); the entire sequence of grids may be repeated (e.g., 2, 2, 4, 4, 8,... , 2, 2, 4, 4, 8,...), and so on. (see Section 4 for examples). These parameters should in fact be optimized for each application according to the concrete needs of the model.

The entire algorithm for the two-dimensional layout correction is summarized below in Algorithm **2D-layout-correction**, where the superscript 0 refers to the current chosen grid size.

2D-layout-correction(graph G, current layout $(\tilde{x}, \tilde{y})$)
begin
   Apply for a sequence of grid sizes
     Construct and initialize $\mathcal{G}^0$, $\mathbf{u}^0$
     Define $\mathcal{C}^0$ to be the set of equidensity constraints
     Initialize the system of equations $\nabla \mathfrak{L}^0$
     V-cycle-correction($\mathcal{G}^0$, $\mathbf{u}^0$, $\mathcal{C}^0$, λ^0, $\nabla \mathfrak{L}^0$)
     Update $(\tilde{x}, \tilde{y})$ from $\mathbf{u}^0$
Return $(\tilde{x}, \tilde{y})$

4. Examples of graph drawing layout correction. As previously mentioned, the graph drawing problem is of interest for many applications. Therefore, we have chosen to demonstrate the abilities of our algorithm for this problem. In this section we will present several results of the two-dimensional layout correction algorithm using inequality constraints. The set of examples is shown in Figures 4.1 and 4.5 to 4.8, each organized in two columns. The initial and final layouts of the graph are shown in the same row, in the left and the right columns, respectively. Note that finalizing the "nice graph" representation of these examples is beyond the scope of this work. The various "beautifying" procedures used by different applications may, of course, be used at the end of our cycles to enhance the visualization results.

The first example consists of a mesh graph with three holes (Figure 4.1, row (a)). It is intended to demonstrate that the empty space stays empty and the energy is thus kept low. More complicated examples are shown in Figure 4.1, rows (b) and (c). The initial optimal positions of the mesh's vertices were randomly changed by independent shifts in different directions within a distance d:

$$d \leq \begin{cases} 2h_x & \text{in example (b)} \\ 4h_x & \text{in example (c)} \end{cases},$$

where h_x is the length of a square on the initially taken 32x32 grid, such that the mesh size of the graph is actually $2h_x$. Let us call these meshes M_1 and M_2, respectively. While the correction of M_1 looks really nice, two switched vertices at the right-hand side of M_2 demonstrate a weak point in our algorithm that certainly must be improved by a local "beautifying" procedure, which in general depends on the real application. The initial layout (c1) is more complicated than (b1), while the desired final layouts are similar.

A typical example of the energy behavior is presented in Figures 4.2-4.4. These figures refer to the mesh example in Figure 4.1-(c). The general energy minimization progress is shown in Figure 4.2. In this example the driving routine alternates between two grid size V-cycles: each odd V-cycle solves the correction problem for the 16x16 grid, while even V-cycles improve the previous iterations with the grid 32x32. Figures 4.3 and 4.4 show the energy behavior of the Window relaxations (without V-cycles) for 16x16 grid iterations and alternately 16x16 and 32x32 grid sizes, respectively. Clearly, the V-cycle algorithm is more powerful in minimizing the energy than just employing the Window relaxations.

A more complicated example is shown in Figure 4.5 in which the 64x64 mesh graph randomly perturbed by vertex shifts (up to $2h_x$ of a 64x64 grid), compressed at the left bottom corner and augmented by 50 randomly chosen edges (Figure 4.5-(a)). The final result of the algorithm is presented in Figure 4.5-(b), where all vertices are placed almost at their optimal locations (note the different scales of the two figures).

We have used 2-FMG cycles with 2 V-cycles at each level as the main driving routine. Such a driving routine works with the following grid sizes: 2, 2, 4, 4, 8, 8, ..., 128, 128, 2, 2, 4, 4, and so forth. After these 2-FMG cycles the total energy was very close to its real minimum and additional iterations have only slightly corrected the layout. The next experiment consists of the 64x64 compressed mesh with three holes. The initial and final layouts are presented in Figures 4.6-(a) and 4.6-(b), respectively.

Two additional examples demonstrate the layout corrections for graphs whose vertices have nonequal volumes (see Figures 4.7 and 4.8). In both cases the initial layout of these graphs was random.

In spite of the promising results presented above, the algorithm has not yet been optimized. However, it is already clear that several parameters must for efficiency be kept very small. For example: (1) the number of *Window relaxation* iterations should be fixed between 1 and 3; (2) "optimal enough" in **SingleWindowSolver** means less than 6 iterations and (3) the size of $\mathcal{W}$ in **SingleWindowSolver** is very robust, that is, the same results can be obtained with sizes 4x4, 8x8, and 16x16. We have used only 4x4 as it runs the fastest.

5. Conclusions. We have presented a linear time multilevel algorithm for solving correction to the nonlinear minimization problem under planar (in)equality constraints. By introducing a sequence of grids over the domain and a new set of global displacement variables defined at those grid points, we formulated the minimization problem under planar equidensity constraints and solved the resulting system of equations by multigrid techniques. This approach enabled fast collective corrections for the optimization objective components. We believe that this formulation can open a new direction for the development of fast algorithms for efficient space utilization goals. Among many possible motivating applications [2, 7, 9, 8, 6, 12, 5, 11, 13] we focused on the demonstration of the method on the graph visualization problem with efficient space utilization demand.

We recommend this multilevel method as a general practical tool in solving, possibly together with other tools, the nonlinear optimization problem under planar (in)equality constraints.

REFERENCES

[1] M. Avriel. *Nonlinear Programming: Analysis and Methods*. Dover Publications, 2003.
[2] G. Di Battista, P. Eades, R. Tamassia, and I. Tollis. *Graph Drawing: Algorithms for the Visualization of Graphs*. Prentice Hall PTR, Upper Saddle River, NJ, USA, 1998.
[3] A. Brandt. Multi-level adaptive solutions to boundary-value problems. *Math. Comp.*, 31(138):333–390, April 1977.
[4] A. Brandt and D. Ron. Chapter 1 : Multigrid solvers and multilevel optimization strategies. In J. Cong and J. R. Shinnerl, editors, *Multilevel Optimization and VLSICAD*, pages 1–69. Kluwer, 2003.
[5] M. Cardei and J. Wu. Energy-efficient coverage problems in wireless ad hoc sensor networks.
[6] Zvi Drezner. *Facility Location: A Survey of Applications and Methods*. Springer, New York, 1995.
[7] P. A. Eades. A heuristic for graph drawing. In *Congressus Numerantium*, volume 42, pages 149–160, 1984.
[8] D. Harel and A. Inger. On the aesthetic layout of higraphs. *submitted*, 2006.
[9] David Harel. On visual formalisms. *Commun. ACM*, 31(5):514–530, 1988.

(a1)   **(a2)**

(b1)   **(b2)**
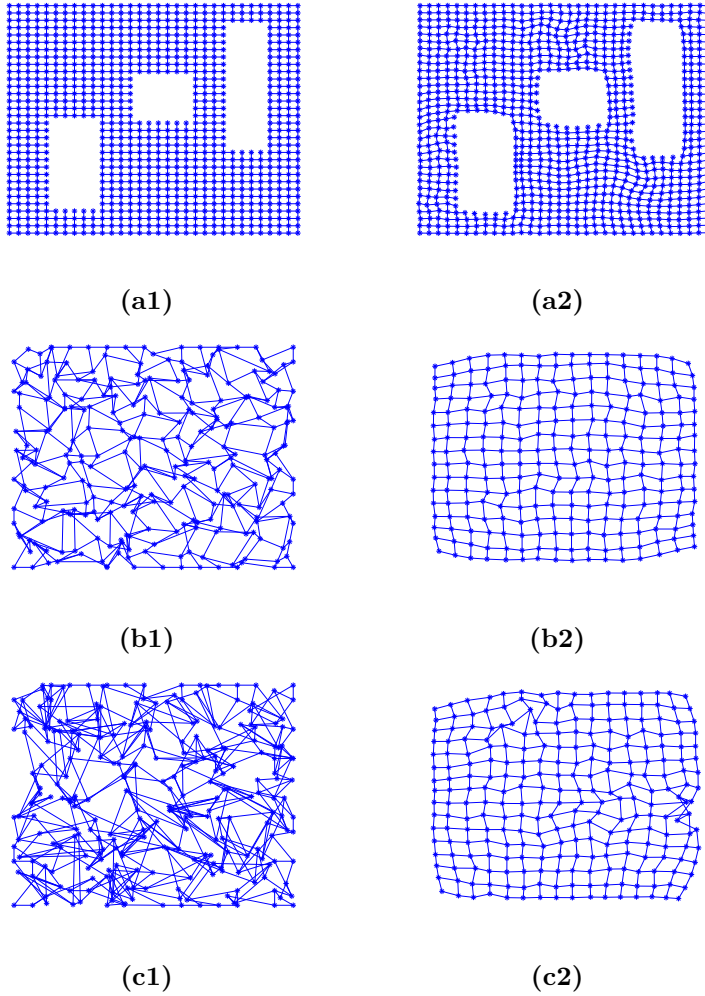
(c1)   **(c2)**

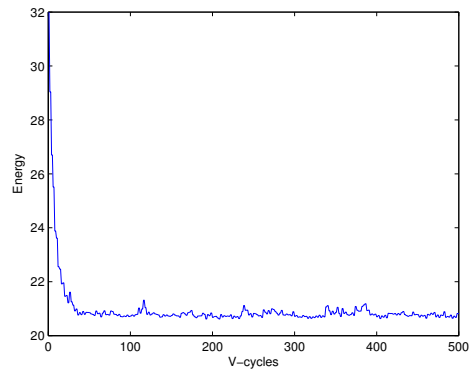FIG. 4.1. *Examples of the 2D-layout of graphs with equal vertices.*

FIG. 4.2. *Energy behavior of the mesh at Figure 4.1-(c), when employing complete V-cycles with 16×16 and 32×32 alternately.*
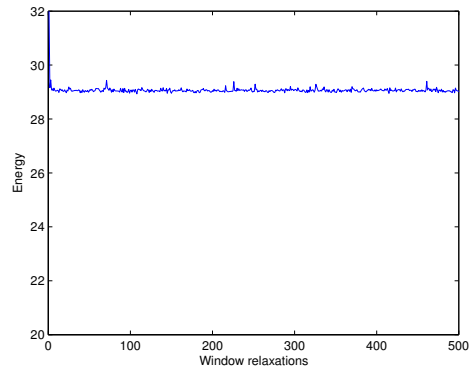
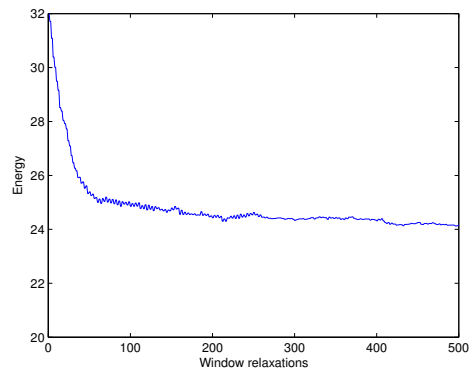FIG. 4.3. *Energy behavior of Window relaxation iterations (16 × 16 grid) of the mesh at Figure 4.1-(c).*

FIG. 4.4. *Energy behavior of Window relaxation iterations (16 × 16 and 32 × 32 grids) of the mesh at Figure 4.1-(c).*

(a) (b)
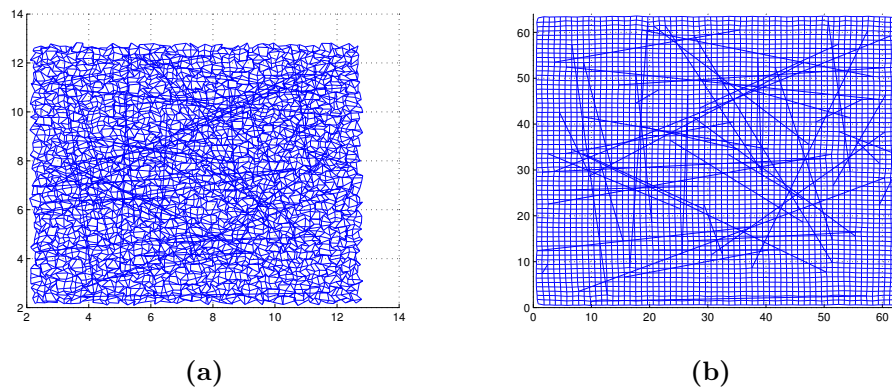
FIG. 4.5. *Example of the layout of the 64 × 64 mesh with additional random edges (note the different scales of the two figures): (a) starting from a compressed and perturbed configuration at the bottom-left corner, (b) the resulting picture using V-cycles.*
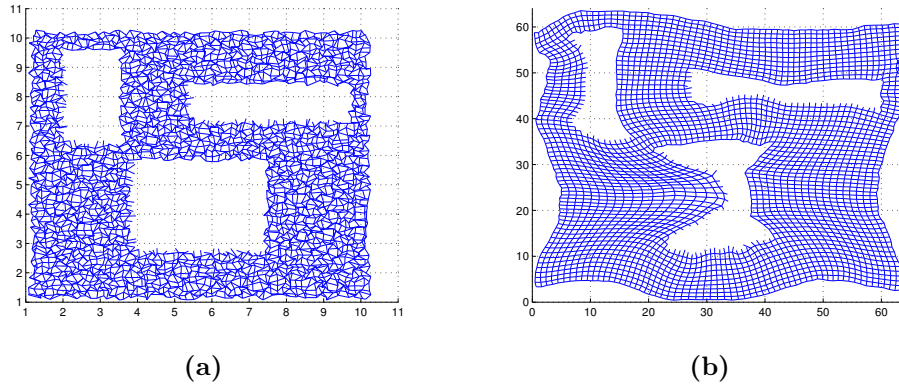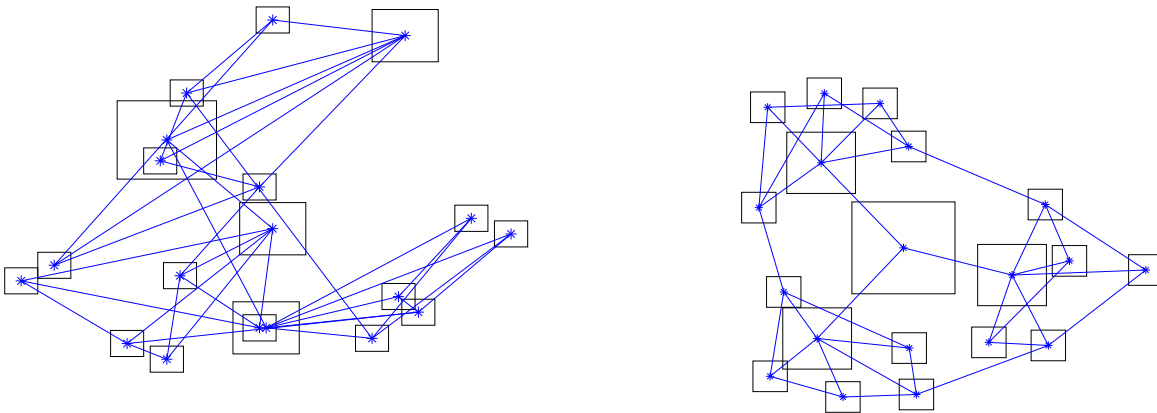
FIG. 4.6. *Example of the* 64×64 *mesh with three holes layout (note the different scales of the two figures): (a) starting from a compressed and perturbed configuration at the bottom-left corner, (b) the resulting picture using V-cycles.*

FIG. 4.7. *Example of the 2D-layout of a graph with nonequal volumes.*

[10] Joe Marks, editor. *Graph Drawing, 8th International Symposium, GD 2000, Colonial Williamsburg, VA, USA, September 20-23, 2000, Proceedings*, volume 1984 of *Lecture Notes in Computer Science*. Springer, 2001.

[11] S. Meguerdichian, F. Koushanfar, M. Potkonjak, and M. B. Srivastava. Coverage problems in wireless ad-hoc sensor networks. volume 3, pages 1380–1387, 2001.

[12] Seapahn Meguerdichian, Farinaz Koushanfar, Miodrag Potkonjak, and Mani B. Srivastava. Coverage problems in wireless ad-hoc sensor networks. In *INFOCOM*, pages 1380–1387, 2001.

[13] G.-J. Nam and J. Cong. *Modern Circuit Placement*. Springer, New York, 2007.

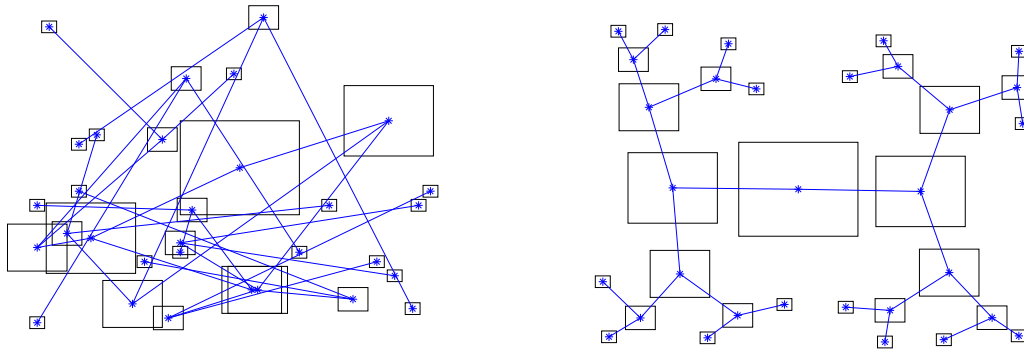[14] U. Trottenberg, C.W. Oosterlee, and A. Schuller. *Multigrid*. Academic Press, Orlando, FL, 2001.

FIG. 4.8. *An example of the 2D-layout of a 5-level binary tree with non-equal vertices.*